SUPPLEMENTAL MATERIAL

Zhang and Hwang, https://doi.org/10.1085/jgp.201611664

According to Scheme S1, the fraction of unblock is calculated with Eq. S1, where [*X*] represents the concentration of $MOPS^-$:

$$O \underset{k_{off}}{\overset{[X]k_{on}}{\rightleftarrows}} O_{blocked} \qquad \text{(Scheme S1)}$$

$$F_{ub} = \frac{1}{1 + \left(\frac{k_{on}}{k_{off}}\right)[X]}. \qquad \text{(S1)}$$

For this two-state model, the binding constant (k_{on}/k_{off}) is the sole determinant deciding the degree of block at a fixed concentration of $MOPS^-$. Therefore, for the mutants with a net charge of 0 (unaltered) or 1, as long as this ratio (k_{on}/k_{off}) is larger for the O_1 state than for the O_2 state, the O_1 state will be more sensitive to $MOPS^-$ block. One can propose that an expansion of the internal vestibule during the O_1 to O_2 transition decreases the electrostatic attraction of the pore for $MOPS^-$, hence resulting in less blockade for the O_2 state. However, for the mutants with a net charge of −1, volume expansion during the O_1 to O_2 transition will decrease the electrostatic "repulsion," resulting in a larger (k_{on}/k_{off}) for the O_2 state compared with that of the O_1 state. At first glance, this prediction contradicts our experimental observation that O_1 and O_2 exhibit equal sensitivity to $MOPS^-$ for these mutants. But if we consider that for mutants with a net charge of −1, the binding constants (k_{on}/k_{off}) for both the O_1 and O_2 states are much smaller than those of WT so that the difference in F_{ub} between the O_1 and O_2 states is too small to be resolved given a dramatic reduction of the single-channel amplitudes of both states (Figs. 2 and 8 D), we can still find proper parameters to fit our data with Scheme S1. However, this model lacks the physical details describing the assigned parameters and is oversimplified for not considering the direct contact between $MOPS^-$ and the wall of the pore. Furthermore, Scheme S1 also implies that the blocking site for $MOPS^-$ is in the internal vestibule. However, the generally held view of a wide space in the internal vestibule argues against a high voltage dependence of the block observed experimentally. After some reckoning, we decided to add one nonconductive docked state for $MOPS^-$ block (Scheme S2 and Fig. S4).

To better explain our data with $MOPS^-$, a "docking" step was introduced into Scheme S1 to derive Scheme S2:

$$O \underset{k_{-1}}{\overset{[X]k_1}{\rightleftarrows}} O_{\text{dock}} \underset{k_{-2}}{\overset{k_2}{\rightleftarrows}} O_{block} \qquad \text{(Scheme S2)}$$

This two-step blocking model is based on the following ideas. First, previous studies using gigantic probes (Zhou et al., 2002; Bai et al., 2011) suggest a wide internal vestibule in CFTR's pore. Thus, if the final destiny for $MOPS^-$ is in this vestibule, the block should not show such a high voltage dependence (Fig. 8) that implicates a residence of the charged head of $MOPS^-$ in a region exhibiting a large voltage drop. Second, the observation that charge manipulations in the internal vestibule do affect $MOPS^-$ block suggests an involvement of the electric field of the internal vestibule in determining $MOPS^-$ block. Third, that part of $MOPS^-$ may be lodged in the deeper part of the internal vestibule is supported by the observation that the F311C mutation, the closest pore-lining residue to the narrow region of the CFTR's pore on TM5 from the cytoplasmic side, increases $MOPS^-$ block (Figs. 8 and 9). Fourth, this two-step blocking scheme has been successfully used to explain the block of CLC-0 chloride channels by organic anions (Zhang and Chen, 2009; Zhang et al., 2009).

The fraction of unblock based on Scheme S2 is described with Eq. S2:

$$F_{ub} = \frac{1}{1 + \left[1 + \left(\frac{k_2}{k_{-2}}\right)\right] \cdot \left(\frac{k_1 \cdot [X]}{k_{-1}}\right)}. \qquad \text{(S2)}$$

Based on this two-step model, kinetic simulations were conducted. One set of parameters that can quantitatively explain the differential responses of our mutants to $MOPS^-$ block are presented in Table S1. Of note, these parameters represent simply one example of results that successfully describe the experimental data from each of the mutation categories. Different sets of parameters can also successfully fit our data as long as (k_1/k_{-1})[*X*] and (k_2/k_{-2}) are not changed drastically.

It is worth noting that if the docking parameters, k_1 and k_{-1}, are voltage independent, we cannot explain mathematically the absence of $MOPS^-$ block at a positive membrane potential (Fig. 8 E). However, as proposed, $MOPS^-$ docks first in the wide internal vestibule that probably does not bear a significant voltage drop. One possibility to resolve this conundrum is that the membrane potential indirectly affects $MOPS^-$ docking by influencing chloride ion occupancy or flow (i.e., trans-ion effects). As the model itself, this explanation remains highly speculative. More experiments are required in the future to accurately incorporate the factor of voltage into our reckoning of the molecular mechanism for differential $MOPS^-$ block in the O_1 and O_2 states.

Importantly, this two-step model of $MOPS^-$ block Scheme S2 can not only quantitatively explain our experimental data through simulations (Table S1) but can also give each parameter its physical meaning, the change of which is accountable by our hypothetic molecular motions of the pore during the O_1 to O_2 transition. As described in the second section of the Discussion, we propose an expansion of the internal vestibule as part of the conformational changes from the O_1 to O_2 state upon ATP hydrolysis. This expansion could in theory weaken the interaction between $MOPS^-$ and the wall of the pore at its blocking site; hence $k_{-2\,(O2)} >> k_{-2\,(O1)}$. However, k_2 is not as sensitive to the size of the pore; hence $k_{2\,(O2)} > k_{2\,(O1)}$. For the docking rate constants, k_1 and k_{-1}, because the docking step reflects diffusion of $MOPS^-$ back and forth between the bulk solution and the internal vestibule, their kinetic constant must be several orders of magnitude higher than those of the blocking step (i.e., k_2 and k_{-2}). However, the exact values of k_1 and k_{-1} will be a function of the electric potential in the internal vestibule: higher k_1 and lower k_{-1} for a favorable potential (0 and 1 in Table S1) relative to the corresponding parameters in an unfavorable condition (−1 in Table S1). Finally, the smaller size of the internal vestibule at the O_1 state will amplify both the favorable and the unfavorable electric potential; for the former, $k_{1\,(O1)} > k_{1\,(O2)}$ and $k_{-1\,(O1)} < k_{-1\,(O2)}$; for the latter, the reverse order or $k_{1\,(O1)} < k_{1\,(O2)}$ and $k_{-1\,(O1)} > k_{-1\,(O2)}$.

In short, Scheme S2 (or Eq. S2) predicts that the degree of $MOPS^-$ block is decided by both docking kinetics (k_1 and k_{-1}) and blocking kinetics (k_2 and k_{-2}). When the electric potential in the internal vestibule is favorable for $MOPS^-$ to dock (0 and 1 in Table S1), both docking and blocking are favored in the O_1 state (and hence a higher degree of block). In contrast, when the electric potential in the internal vestibule is unfavorable for docking of $MOPS^-$ (−1 in Table S1), this disfavored electric potential is exaggerated in the O_1 state, and the resulting dampened docking kinetics effectively cancels out the favorable blocking kinetics of the O_1 state.

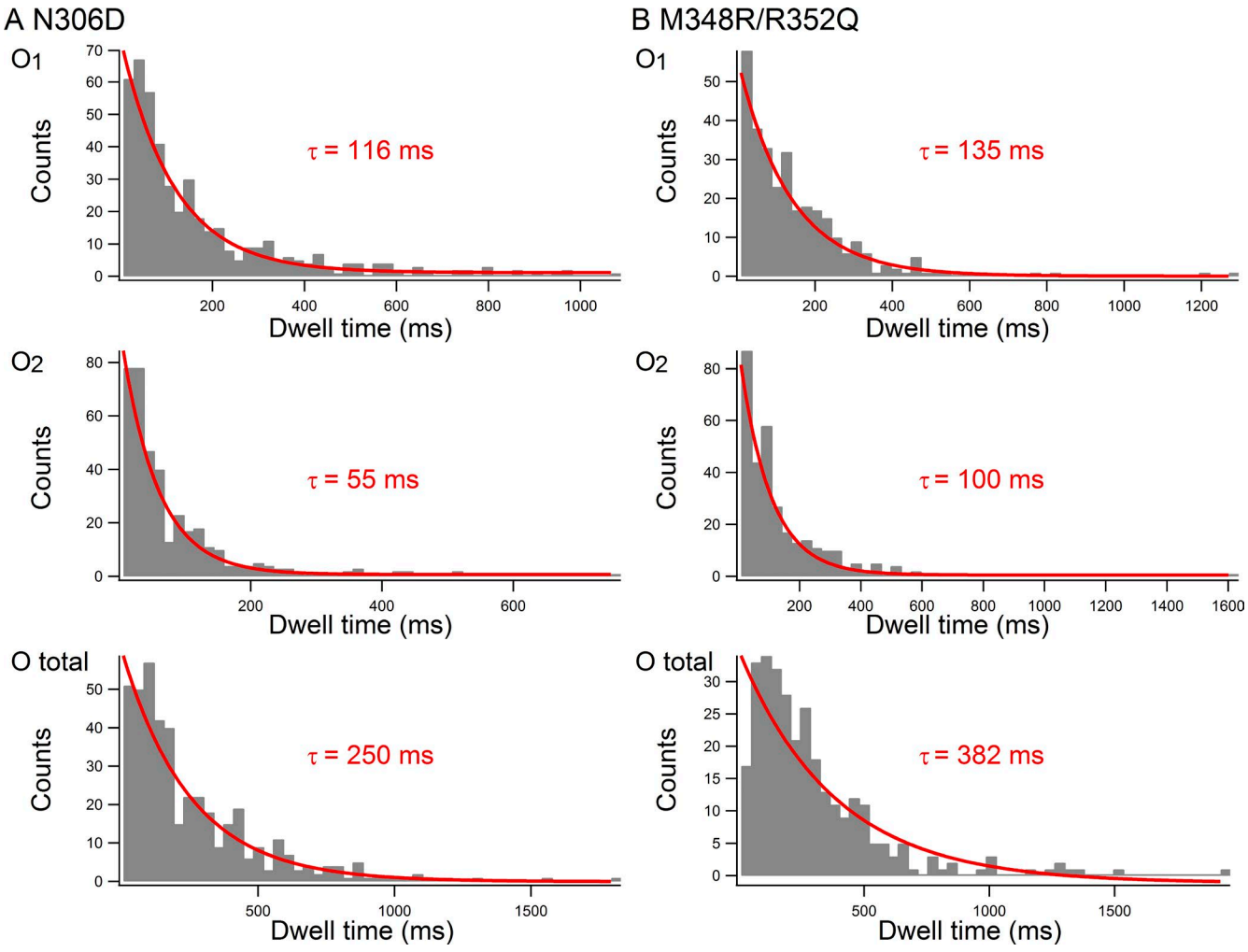

Figure S1. **Dwell-time histograms for the O_1 state, O_2 state, and opening burst in N306D and M348R/R352Q.** All histograms can be fitted well with a single-exponential function (time constants are indicated). As the time constants for the O_2 state are several-fold larger than the 8-ms cutoff used to identify a state, missed events are not a major problem in our statistical analysis of the gating topology.

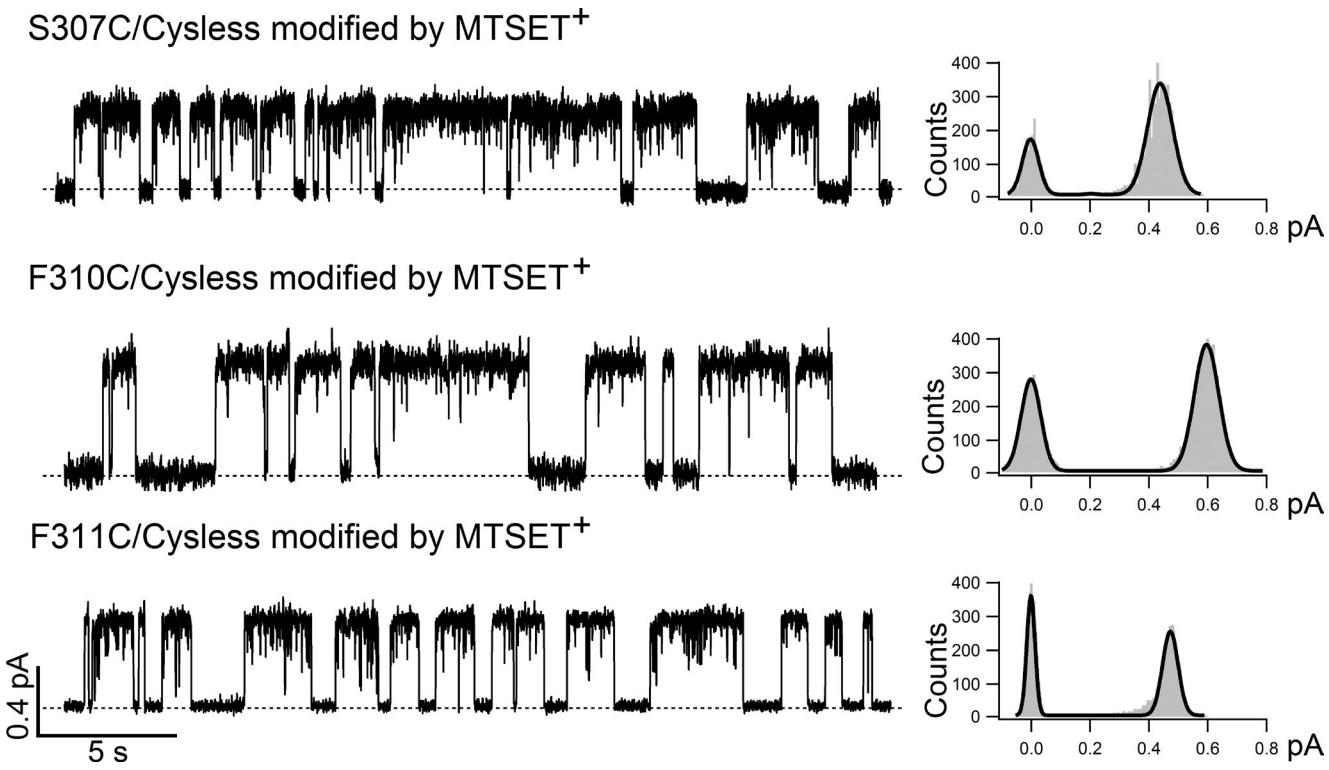

Figure S2. **S307C/Cysless, F310C/Cysless, and F311C/Cysless modified by MTSET$^+$ show only one single-channel conductance level.** Each all-point histogram of the open-channel level can be fitted with a single Gaussian function. Compared with Fig. 5, the data here suggest that adding one additional positive charge at S307, F3110, or F311 does not yield the O_1O_2 phenotype; the simultaneous neutralization of R303 is also required for the presence of the O_1O_2 phenotype, supporting the critical role of the position of charges in determining the O_1O_2 phenotype.

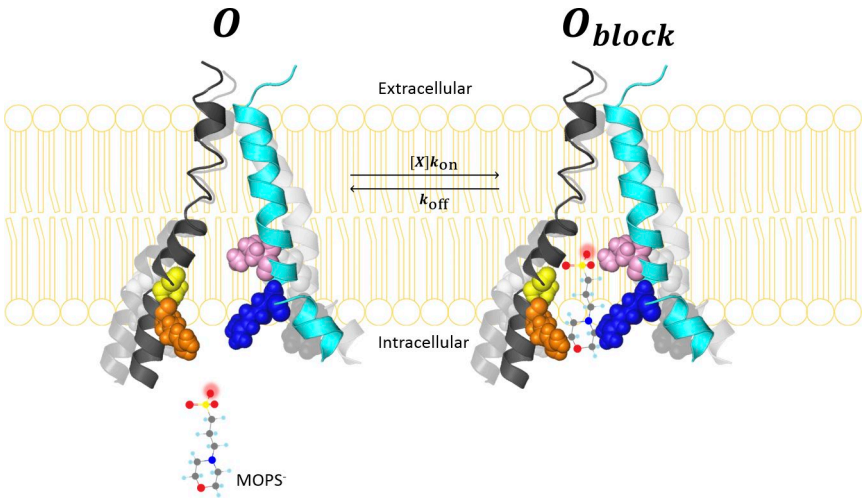

Figure S3. **Two-state model for differential MOPS$^-$ block between the O_1 and O_2 states.** The color code is the same as that in Fig. 10. The negative head of MOPS$^-$ is highlighted with red shadow. The transmembrane segments in this figure and in Fig. S4 are extracted from the homology model published by Dalton et al. (2012). The mechanism behind the charge-dependent differential sensitivities of the O_1 state and O_2 state to the application of the channel-impermeant blocker MOPS$^-$ can be explained by a simple canonical one-step blocking scheme.

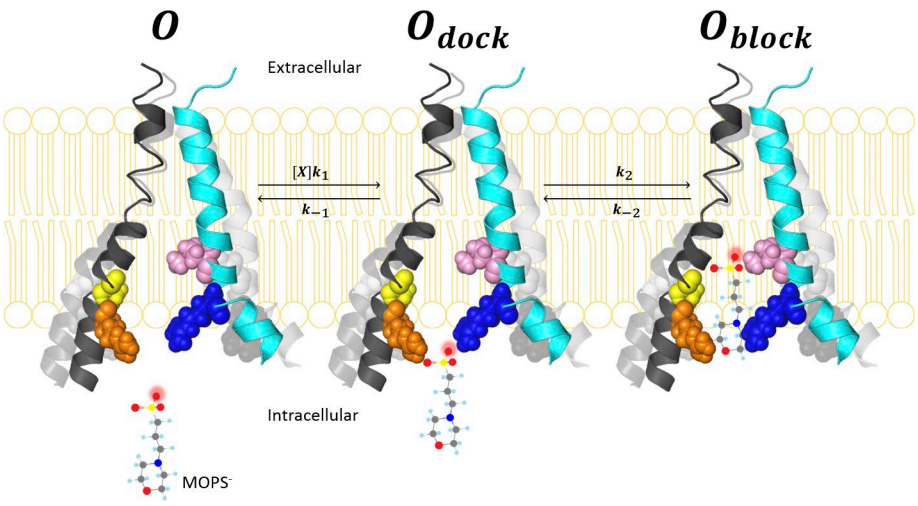

Figure S4. **Three-state model for $MOPS^-$ block.** The color code is the same as that in Fig. 10.

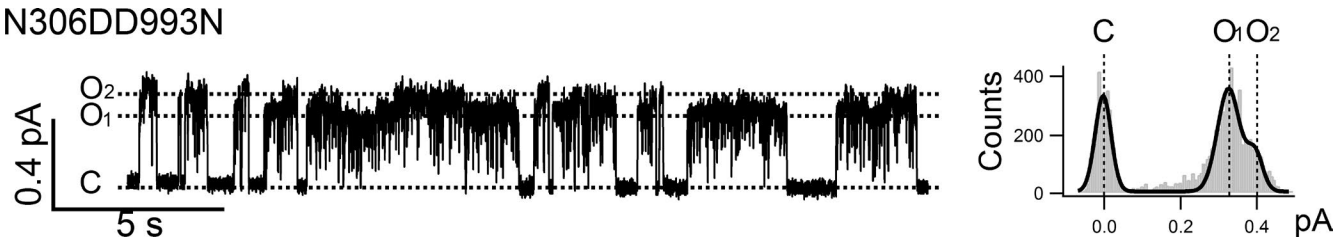

Figure S5. **Neutralization of D993 affects the O_1O_2 phenotype in N306D.** A representative single-channel trace (left) shows the double mutant N306D/D993N displaying two distinct open-channel current amplitudes: O_1 (0.32 ± 0.01 pA, n = 3) and O_2 (0.39 ± 0.01 pA, n = 3). The corresponding all-points histogram (right) barely shows an additional peak to the right of the main peak of the O_1 state. Compared with the single mutant N306D (O_1: 0.18 ± 0.01, n = 3; and O_2: 0.24 ± 0.01, n = 3), neutralizing the aspartate at position 993 under the N306D background increases the single-channel amplitudes of both O_1 and O_2 states but decreases the relative difference in single-channel amplitude between these two states as if D306 can partially replace the function of D993. These results are consistent with the idea that there is a superposition of electric fields produced by the charge at positions 306 and 993, presumably because of a physical proximity.

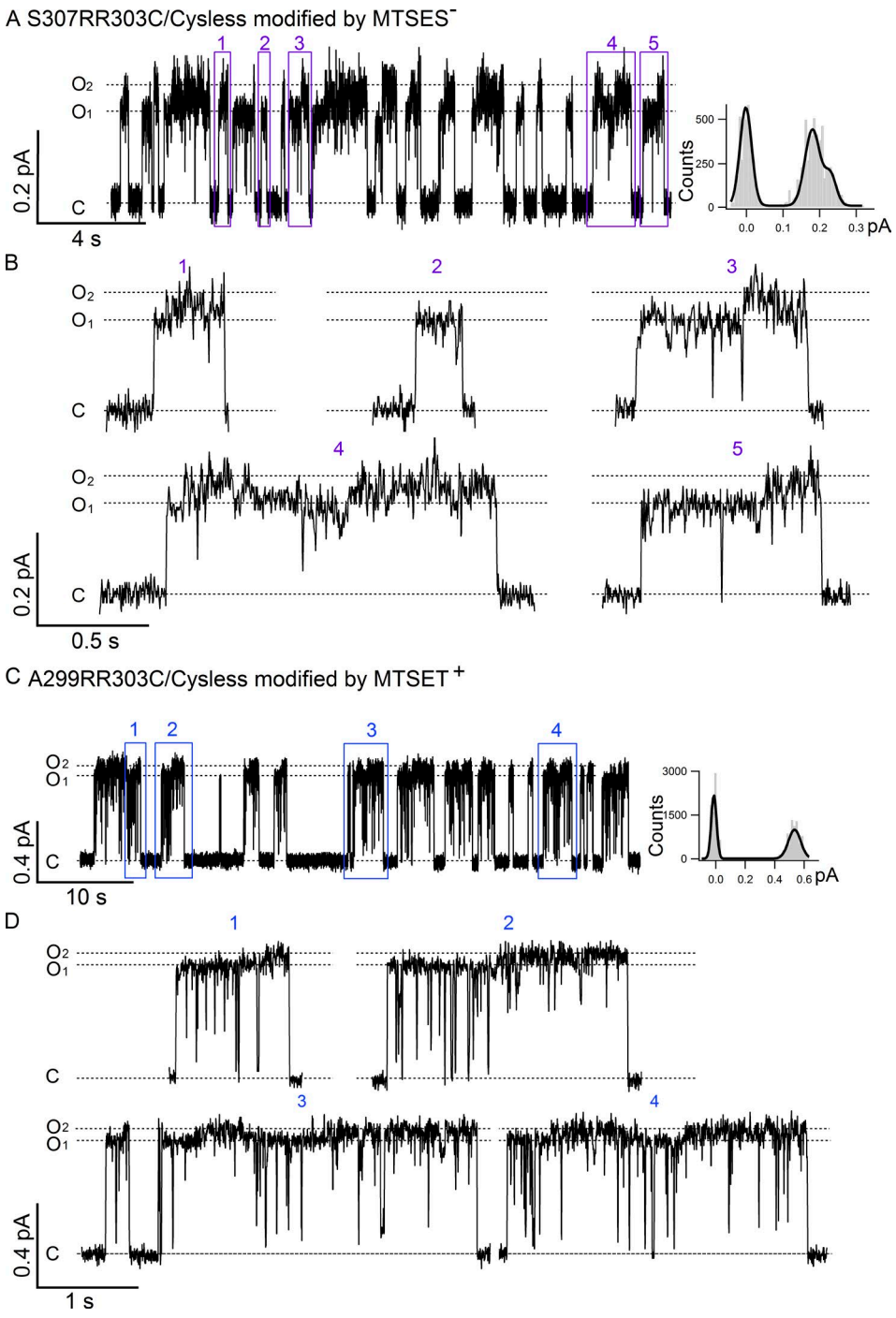

Figure S6. **Modification of S307R/R303C/Cysless and A299R/R303C/Cysless changes their phenotype.** (A) S307R/R303C/Cysless modified by negatively charged thiol-specific reagent $MTSES^-$ displays a clear O_1O_2 phenotype (O_1: 0.17 ± 0.01, n = 3; and O_2: 0.23 ± 0.01, n = 3), whereas the S307R/R303C/Cysless itself (Fig. 5 A) does not show a clear difference in single-channel amplitudes between its O_1 and O_2 states. (B) Expanded bursts marked in A show details of each opening burst and the preferred gating transition of $C \rightarrow O_1 \rightarrow O_2 \rightarrow C$ for bursts 3–5. The single-channel behaviors of S307R/R303C/Cysless before (Fig. 5) and after $MTSES^-$ modification support the ideas that ion permeation through the internal vestibule of CFTR's pore has to be delicately tuned through the cooperation between multiple pore-lining residues placed at specific locations such as 303, 306, 307, 352, and 348 and that the functional perturbations caused by mutations at these positions are amplified in the O_1 state, resulting in the O_1O_2 phenotype. (C) A299R/R303C/Cysless modified by the positively charged thiol-specific reagent $MTSET^+$ displays a clear O_1O_2 phenotype, although with a small difference between two open states (O_1: 0.47 ± 0.02, n = 4; and O_2: 0.52 ± 0.02, n = 4). (D) Expanded bursts marked in C show details of the O_1 to O_2 transitions.

Table S1. **A sample set of simulation parameters using the two-step scheme for $MOPS^-$ block**

Net charge	State	$[X]\cdot k_1$	k_{-1}	k_2	k_{-2}	F_{ub}
0, 1 (WT, A299R, F311C/Cysless)	O_1	100,000	120,000	200	50	0.19
	O_2	80,000	140,000	300	200	0.41
−1 (N306D, R303C/Cysless)	O_1	40,000	600,000	400	50	0.63
	O_2	50,000	400,000	600	200	0.67

Electropositivity order in the internal vestibule (from positive to negative): $O_{1(0,+1)} > O_{2(0,+1)} > O_{2(-1)} > O_{1(-1)}$. Order of $[X]\cdot k_1$: $O_{1(0,+1)} > O_{2(0,+1)} > O_{2(-1)} > O_{1(-1)}$. Order of k_1: $O_{1(0,+1)} < O_{2(0,+1)} < O_{2(-1)} < O_{1(-1)}$. So that the order of $[X]\cdot k_1/k_1$: $O_{1(0,+1)} > O_{2(0,+1)} >> O_{2(-1)} > O_{1(-1)}$.

REFERENCES

Bai, Y., M. Li, and T.C. Hwang. 2011. Structural basis for the channel function of a degraded ABC transporter, CFTR (ABCC7). *J. Gen. Physiol.* 138:495–507. http://dx.doi.org/10.1085/jgp.201110705

Dalton, J., O. Kalid, M. Schushan, N. Ben-Tal, and J. Villà-Freixa. 2012. New model of cystic fibrosis transmembrane conductance regulator proposes active channel-like conformation. *J. Chem. Inf. Model.* 52:1842–1853. http://dx.doi.org/10.1021/ci2005884

Zhang, X.D., and T.Y. Chen. 2009. Amphiphilic blockers punch through a mutant CLC-0 pore. *J. Gen. Physiol.* 133:59–68. http://dx.doi.org/10.1085/jgp.200810005

Zhang, X.D., P.Y. Tseng, W.P. Yu, and T.Y. Chen. 2009. Blocking pore-open mutants of CLC-0 by amphiphilic blockers. *J. Gen. Physiol.* 133:43–58. http://dx.doi.org/10.1085/jgp.200810004

Zhou, Z., S. Hu, and T.C. Hwang. 2002. Probing an open CFTR pore with organic anion blockers. *J. Gen. Physiol.* 120:647–662. http://dx.doi.org/10.1085/jgp.20028685